THE ASTROPHYSICAL JOURNAL, 555:967–977, 2001 July 10

PHASE-DEPENDENT SPECTRAL VARIABILITY IN 4U 1907+09

MALLORY S. E. ROBERTS[1] AND PETER F. MICHELSON
Department of Physics, Stanford University, 382 Via Puebla Mall, Stanford, CA 94305; mallory@astro.stanford.edu, peterm@leland.stanford.edu

DENIS A. LEAHY
Department of Physics, University of Calgary, 2500 University Drive, NW, Calgary, AB T2N 1N4, Canada; leahy@iras.ucalgary.ca

TONY A. HALL[2] AND JOHN P. FINLEY
Department of Physics, Purdue University, 1396 Physics Building, West Lafayette, IN 47907; hall@egret.sao.arizona.edu, finley@physics.purdue.edu

LYNN R. COMINSKY
Department of Physics and Astronomy, Sonoma State University, 1801 East Cotati Avenue, Rohnert Park, CA 94928; lynnc@charmian.sonoma.edu

AND

RADHIKA SRINIVASAN
Department of Radiology/MRSC, University of California at San Francisco, 505 Parnassus Avenue, Box 0629, San Francisco, CA 94143; rsriniva@mrsc.ucsf.edu

Received 2000 April 14; accepted 2001 March 8

ABSTRACT

We report on *ASCA*, *RXTE*, and archival observations of the high-mass X-ray binary pulsar 4U 1907+09. Spectral measurements of the absorption and flux were made at all phases of the X-ray pulsar orbit, including the first spectral measurements of an extended period of low flux during two of the *ASCA* observations. We find that a simple spherical wind model can fit the time-averaged light curve as measured by the *RXTE* All-Sky Monitor but does not fit the observed changes in the absorption column or account for the existence of the phase-locked secondary flare. An additional model component consisting of a trailing stream can account for the variations in column depth. However, these models favor a high inclination angle for the system, suggesting a companion mass more consistent with an identification as a Be star. In this case, an equatorially enhanced wind and inclined neutron star orbit may be a more appropriate interpretation of the data.

Subject headings: pulsars: individual (4U 1907+09) — stars: emission-line, Be — stars: mass loss — X-rays: stars

1. INTRODUCTION

4U 1907+09 was noted as a variable X-ray source during the early sky surveys with *Uhuru* (Giacconi et al. 1971), *Ariel 5* (Seward et al. 1976), *OSO 7* (Markert et al. 1979), and *HEAO 1* (Schwartz et al. 1980). The latter allowed Schwartz et al. (1980) to identify the source with a heavily reddened $m_v \simeq 16.4$ star having a broad Hα emission line, which they assumed was an OB supergiant. A large X-ray outburst observed by *Ariel 5* during 1980 January indicated regular flux modulation on a timescale of days. Further analysis of all the *Ariel 5* data revealed a period of 8.4 days (Marshall & Rickets 1980). The folded period profile shows a large primary peak as well as a smaller secondary maximum roughly half a cycle later. Long-term observations by *Vela 5B* seemed to indicate an additional quasi periodicity at $P \sim 41.6$ days, which was proposed to be due to precession similar to that of Her X-1 (Priedhorsky & Terrell 1984).

In 1983 *Tenma* observed 4U 1907+09 for an entire 8 day cycle, which resulted in the discovery of double-peaked 437.5 s pulsations (Makishima et al. 1984). Analysis of the pulse arrival times allowed an estimate of the orbital parameters to be made, which confirmed the 8.38 day period as the orbital period. A moderately eccentric ($e \sim 0.22$) orbit best fitted the data, although a circular orbit also provided an adequate fit. Makishima et al. also determined a mass function of $\sim 9\ M_\odot$, confirming the massive nature of the companion. Further observations by *EXOSAT* (Cook & Page 1987) implied a mean spin-down rate of ~ 0.23 s yr^{-1} and a variable column density [$(1.5–5.7) \times 10^{22}$ cm^{-2}] and slightly refined the *Tenma* orbital elements. The observed spectra were consistent with a hard power law ($\alpha \sim 1.2$) with a variable low-energy cutoff. Balloon observations of 4U 1907+09 in the 20–100 keV range and analysis of *Einstein* archival data are consistent with the *EXOSAT* spectral observations (Chitnis et al. 1993).

Ginga spectral studies suggested a cyclotron absorption feature at ~ 19 keV (Mihara 1995; Makishima et al. 1999), which has been confirmed by a recent *BeppoSAX* observation (Cusumano et al. 1998), along with the discovery of the second harmonic at 39 keV, suggesting a surface magnetic field strength of $\sim 2 \times 10^{12}$ G. An iron emission line at ~ 6.4 keV was also detected with an equivalent width of ~ 60 eV. A pulse period of $\sim 439.5 \pm 0.6$ s is clearly seen in the *Ginga* data during most of the observations, in which the source had an average intensity of 15–20 mcrab. However, 4U 1907+09 also exhibited extended periods of weaker intensity (~ 3 mcrab) accompanied by a reduced pulsed fraction (Makishima et al. 1999).

Iye (1986) performed the first detailed spectroscopic studies of the companion star to 4U 1907+09. He concluded, in contrast to the initial assumptions by Schwartz et al. (1980), that the spectral type of the companion was B2 III–Ve and that the two X-ray flares seen in some orbits were due to the intersection and subsequent accretion of material in an extended disk around the companion by the orbiting neutron star.

[1] McGill University, Physics Department, 3600 University Street, Montreal, QC H3A 2T8, Canada.
[2] Iowa State University c/o Smithsonian Institution, Steward Observatory, 933 North Cherry Avenue, Tucson, AZ 85719.

Van Kerkwijk, van Oijen, & van den Heuvel (1989) next undertook extensive spectroscopic studies to determine whether the companion to 4U 1907+09 is an OB supergiant or a Be star. They considered X-ray, optical, and orbital data and suggested that most of the measurements support the supergiant nature of the companion, including the reddening and distance, Hα FWHM, and rotation velocity of the companion. In addition, the location of 4U 1907+09 in the spin period versus orbital period diagram (Corbet 1984) is inconsistent with the trend observed for most Be/X-ray pulsars, suggesting instead a wind-fed supergiant system. Since it is difficult to produce a phase-locked secondary flare from the wind of a supergiant star, van Kerkwijk et al. (1989) suggested that the secondary flare may be spurious in nature. There is one clear case of a wind-fed supergiant/X-ray pulsar system, GX 301−2, that has a tendency to flare twice per orbit for extended periods of time (Pravdo et al. 1995), but the cause of this is not well understood.

Recent observations of 4U 1907+09 with *RXTE* showed highly variable flux with frequent drops to below the detection threshold (in 't Zand, Strohmayer, & Baykal 1997). There is no evidence for increased absorption during the drops in their data, suggesting that the low-flux levels are due to a low accretion rate. A possible flare that is consistent in phase with previously observed secondary flares was also seen in the *RXTE* data. The 2–30 keV *RXTE* spectrum is well fitted by a cutoff power law having a photon index $\alpha \sim 1.0$–1.3 with a cutoff energy of 13.6 keV and $N_{\rm H}$ varying from 1×10^{22} to 9×10^{22} cm^{-2}, with the lowest values occurring during the secondary flare. No evidence for line emission was found with an $\sim$60 eV upper limit on an iron line equivalent width.

By combining the *RXTE* data with the *Tenma* data, in 't Zand, Baykal, & Strohmayer (1998) obtained a slightly improved orbital fit. This allowed a good determination of the orbital period (8.3753 ± 0.0003 days). However, the eccentricity is still not well determined, with a 68% confidence region of 0.14–0.38. They also reported the discovery of 18 s oscillations during a 1 hr flare, which may be the result of the beat frequency between the spin period and an accretion disk. In addition, the measured spin period $P_s = 440.341^{+0.012}_{-0.017}$ suggests that the pulsar has been steadily spinning down since 1983, with $\dot{P}_s = +0.225$ s yr^{-1}.

In this paper we present timing and spectral analysis of four *ASCA* observations of 4U 1907+09 and spectral analysis of an additional nine *RXTE* observations, roughly equally spaced around the 8.4 day orbit. We also report on archival observations of this source with *HEAO 1* A-1 and the *RXTE* All-Sky Monitor (ASM). We then compare these and all previous observations of 4U 1907+09 to a model of accretion from a spherical wind coming from the companion.

2. ARCHIVAL OBSERVATIONS

We have investigated archival *HEAO 1* A-1 scanning data on 4U 1907+09. *HEAO 1* A-1 observed 4U 1907+09 in a series of 32 s scans during 1978 April 7–14. The data show orbital behavior consistent with the *Tenma*/*EXOSAT* period, with two peaks at orbital phases consistent with what was seen by *Ariel 5*. The light curve from the A-1 observations is shown in Figure 1.

The *RXTE* ASM has been observing this source since it began regular observations in 1996 February. We report here on $\sim$1400 days of data (MJD 50,136–51,549). Errors on individual flux measurements are relatively large, making examinations on timescales of days unreliable. However, epoch-folding of the light curve clearly shows the orbital modulation. In Figure 2 we show the average orbital light curve for the entire data set, with the orbital period and epoch $T_{\pi/2}$ from in 't Zand et al. (1998). The vertical lines represent the 68% confidence region at the time of periastron. There is evidence for a secondary flare at a phase

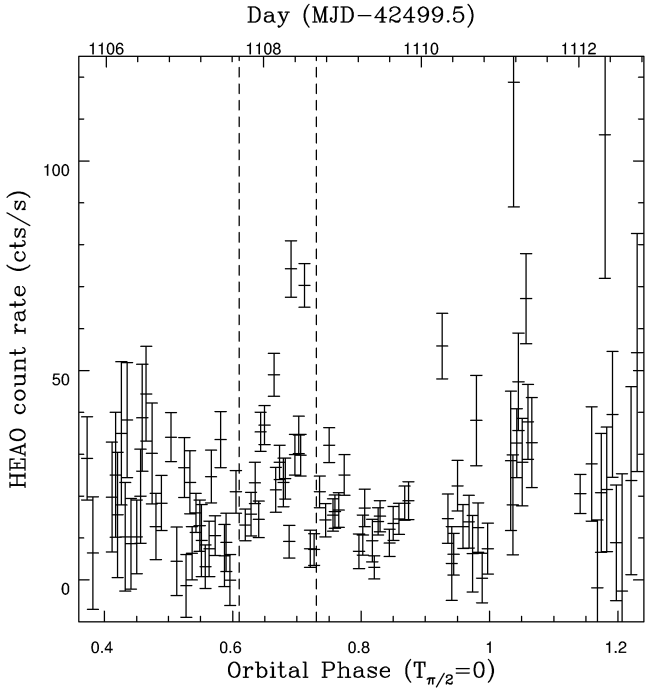

FIG. 1.—Light curve of 4U 1907+09 during the 1978 *HEAO 1* A-1 observations. The vertical lines in this and the following figures represent the 68% confidence region of the time of periastron.

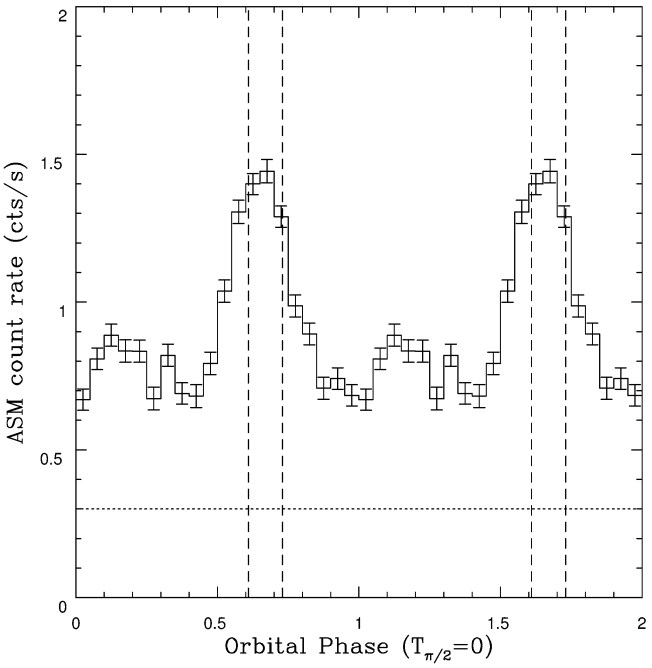

FIG. 2.—*RXTE* ASM light curve of the 8.3753 day orbital period averaged over the 4 yr data set. The dotted line is the level of positive flux bias assumed for later model fits.

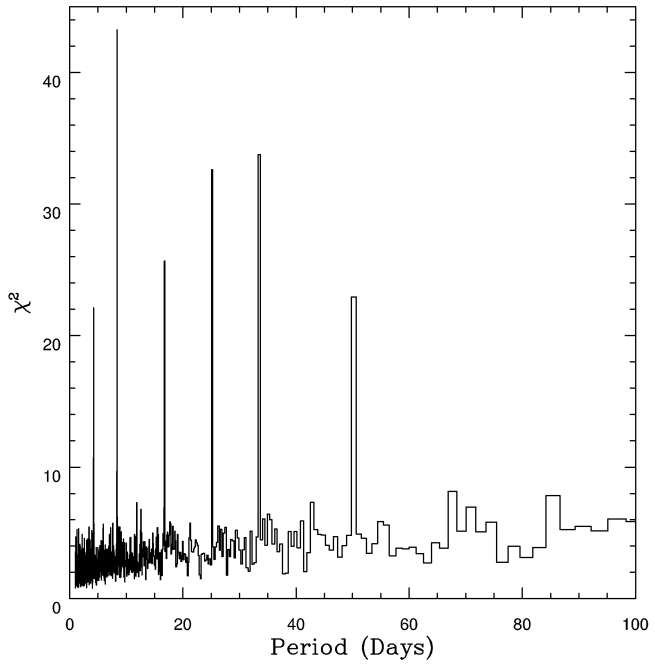

FIG. 3.—Period search of the *RXTE* ASM data showing the 8.4 day orbital period and multiples.

of ~0.15. We also folded separately the light curves from the three energy channels (1.3–3.0, 3.0–5.0, and 5.0–12.1 keV) of the ASM and found evidence for the secondary flare at a consistent phase in each. A comparison of the first half of the data set to the second showed that this is a fairly stable feature. The ratio of the flare to the quiescent flux is difficult to estimate since there is known to be a positive flux bias in the ASM data. In the case of 4U 1907+09, this bias is exacerbated by several nearby sources including GRS 1915+105 and W49B.

We have also performed a period search on the ASM data in order to search for other periodicities such as the proposed 41 day periodicity (Priedhorsky & Terrell 1984). We binned the data into 20 phase bins and calculated χ^2_ν for a constant model-averaging over phase, as recommended by Collura et al. (1987). As Figure 3 shows, the 8.375 day orbital period and several multiples of it are poorly fitted by a constant model. Although not evident in the ASM data folding, 5 times the orbital period would correspond to 41.9 days, which is consistent with the quasi periodicity seen in the *Vela 5B* data by Priedhorsky & Terrell (1984) and interpreted as an additional, longer period. We find no evidence for a periodicity in the long-term light curve of this system, which is unrelated to the orbital period.

3. *ASCA* OBSERVATIONS

In 1996 August, *ASCA* made four 10 ks observations of 4U 1907+09, roughly equally spaced throughout the 8.4 day orbit. Observational parameters are listed in Table 1. Extraction regions of a 6′ radius were used for the Gas Imaging Spectrometer (GIS) detectors, while a 4′ radius was used for the Solid-State Imaging Spectrometer 0 (SIS0). A slightly smaller region was used for SIS1 (~3′.5) since the source was nearer to the edge of the chip. Since the source is in the galactic ridge, a local estimate of the background is necessary. Therefore, source-free regions of the detectors were used for extracting background light curves and spectra with a background rate of $\sim 3 \times 10^{-2}$ counts s^{-1} in each detector.

3.1. *Temporal Analysis*

The background-subtracted GIS3 light curves for all four observations (Aobs 1–4) are shown in Figure 4. Aobs 1 consists of short flaring episodes with times of low flux in between where the count rate dropped by a factor of ~10, reminiscent of the "dipping" seen in the earlier *RXTE* observations (in 't Zand et al. 1997). Aobs 2 and Aobs 3 show the source in a very low state, a factor of ~50 below the average flux in Aobs 4 and a factor of ~4 below the low-flux states in Aobs 1. Since Aobs 4 has the best statistics and is relatively constant on timescales longer than the pulse period, we used it to find the best pulse period of 440.35 ± 0.06 s (after correcting the arrival times for the orbital motion of the pulsar, assuming the orbital parameters of in 't Zand et al. 1998) by epoch-folding the light curve. We then folded each of the observations at this period and show these in Figure 5. The pulses seem to

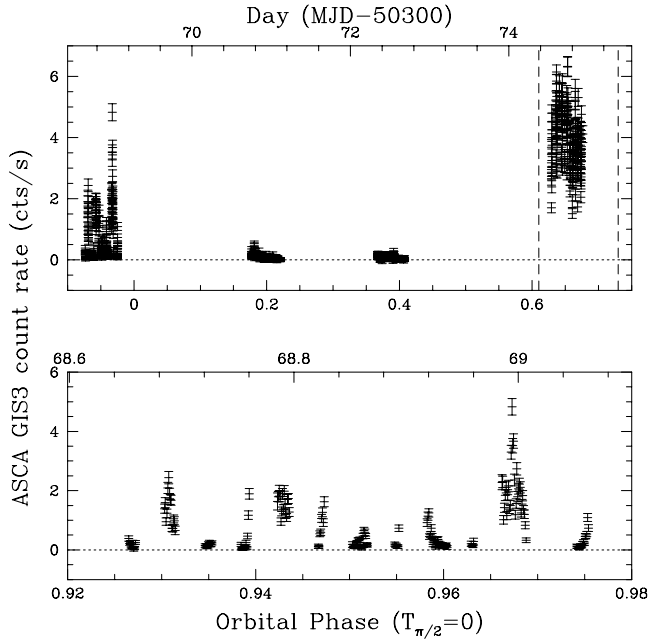

FIG. 4.—*ASCA* GIS light curve of the four observations of 4U 1907+09 (*upper panel*) and of Aobs 1 alone (*lower panel*).

TABLE 1

ASCA OBSERVATION PARAMETERS

Observation	Sequence ID	Date (MJD −50,300)	Orbital Phase ($T_{\pi/2}=0$)	On Time (ks)	Mean GIS Rate (counts s^{-1})
Aobs 1.....	44020040	68.65–69.06	0.93–0.98	10.2	0.702 ± 0.008
Aobs 2.....	44020010	70.75–71.12	0.18–0.22	10.1	0.067 ± 0.005
Aobs 3.....	44020020	72.34–72.53	0.37–0.39	9.3	0.064 ± 0.005
Aobs 4.....	44020030	74.54–74.94	0.63–0.68	9.9	3.447 ± 0.015

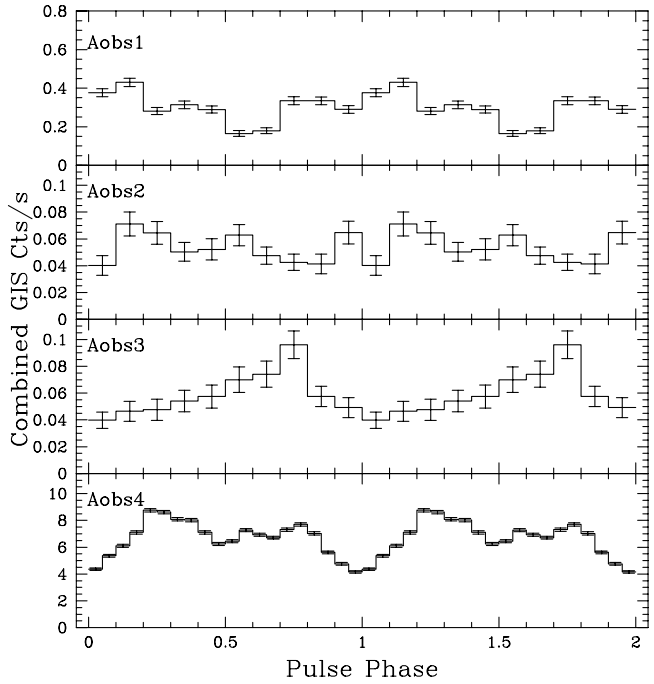

FIG. 5.—Pulse profiles from the *ASCA* observations. The photon arrival times are corrected for the pulsar orbit and folded from a common epoch using the best-fit period of 440.35 s from epoch-folding Aobs 4. The error in the period results in a relative phase uncertainty between Aobs 1 and Aobs 4 of ~0.15.

change shape and become weaker during the low states (Aobs 2 and Aobs 3).

3.2. *Orbital Phase Spectroscopy*

Using XSELECT, spectra were extracted from each of the four detectors for each observation. These were analyzed using XSPEC and fitted to an absorbed power-law model and narrow ($\sigma = 0$) Gaussian lines were added if they significantly improved the fit. Aobs 2 and Aobs 3 had very low statistics, so the two GIS detectors were combined into one data set, as were the two from the SIS detectors. In order to use all available photons, SIS Bright mode data were used. The results are shown in Table 2. It can immediately be seen that the lower states (Aobs 2 and Aobs 3) show no evidence of increased absorption. The lowest absorption occurs during Aobs 4, the brightest observation, and is a factor of 2 lower than the high absorption seen during Aobs 1. The spectral slope changes by a small, but statistically significant, amount. Weak iron line emission is present during Aobs 4 and may be present during the other observations, although the statistics were not good enough to give more than upper limits at the 90% confidence level.

In order to test whether the drops in flux during Aobs 1 are due to an increase of column depth, we extracted spectra separately from the flaring and the low portions of the data set. As shown in Figure 6, there is no evidence of increased absorption during dips. In fact, there is evidence that the

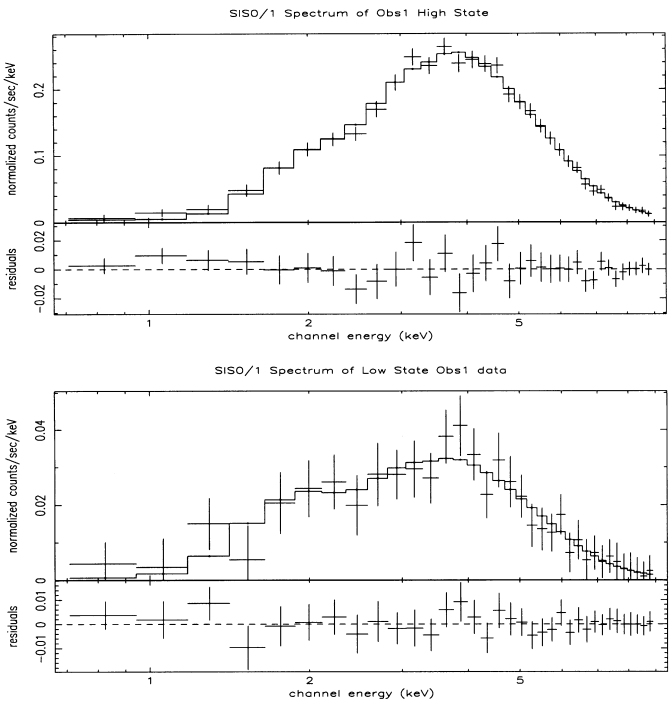

FIG. 6.—High-state and low-state SIS energy spectra for Aobs 1

TABLE 2

ASCA SPECTRAL FITS

Observation	n_H ($\times 10^{22}$ cm^{-2})	Γ	Line Energy (keV)	Line Equivalent Width (eV)	$F_{2-10\,keV}$ ($\times 10^{-10}$ ergs cm^{-2} s^{-1})	χ^2_ν (dof)
Fits from GIS2 + GIS3						
Aobs 1.....	$3.89^{+0.37}_{-0.36}$	$1.02^{+0.12}_{-0.12}$	$6.53^{+0.32}_{-0.52}$	76 ± 33	1.11 ± 0.02	0.58 (38)
Aobs 1 hi.....	$4.18^{+0.41}_{-0.38}$	$1.05^{+0.13}_{-0.12}$	$6.45^{+0.31}_{-0.22}$	82 ± 33	1.73 ± 0.02	0.50 (38)
Aobs 1 lo.....	$2.12^{+1.68}_{-1.12}$	$0.92^{+0.67}_{-0.53}$	...	...	0.23 ± 0.02	0.24 (40)
Aobs 2.....	$2.59^{+1.44}_{-1.07}$	$2.07^{+0.81}_{-0.65}$	...	...	0.066 ± 0.005	0.25 (40)
Aobs 3.....	$2.70^{+1.71}_{-1.28}$	$1.93^{+0.88}_{-0.73}$	...	...	0.066 ± 0.005	0.19 (40)
Aobs 4.....	$1.74^{+0.06}_{-0.06}$	$1.23^{+0.04}_{-0.03}$	$6.53^{+0.11}_{-0.11}$	79 ± 16	4.20 ± 0.02	1.71 (38)
Fits from SIS0 + SIS1						
Aobs 1.....	$3.83^{+0.39}_{-0.36}$	$1.03^{+0.14}_{-0.14}$	6.34 (frozen)	<57.1	0.87 ± 0.01	0.53 (289)
Aobs 1 hi.....	$4.01^{+0.42}_{-0.39}$	$1.04^{+0.14}_{-0.15}$	6.34 (frozen)	<65.8	1.42 ± 0.02	0.51 (289)
Aobs 1 lo.....	$2.47^{+1.72}_{-1.20}$	$0.96^{+0.69}_{-0.60}$	...	...	0.18 ± 0.01	0.35 (35)
Aobs 2.....	$2.50^{+1.28}_{-0.93}$	$1.89^{+0.78}_{-0.64}$	...	...	0.051 ± 0.003	0.30 (28)
Aobs 3.....	$1.85^{+1.23}_{-0.84}$	$1.34^{+0.72}_{-0.59}$	...	...	0.063 ± 0.004	0.19 (28)
Aobs 4.....	$1.87^{+0.05}_{-0.06}$	$1.35^{+0.04}_{-0.04}$	$6.34^{+0.08}_{-0.08}$	70.0 ± 15.8	3.49 ± 0.02	0.83 (324)

NOTE.—Errors with separate plus and minus values represent 9% multiparameter confidence regions. Errors with a single value are 1 σ.

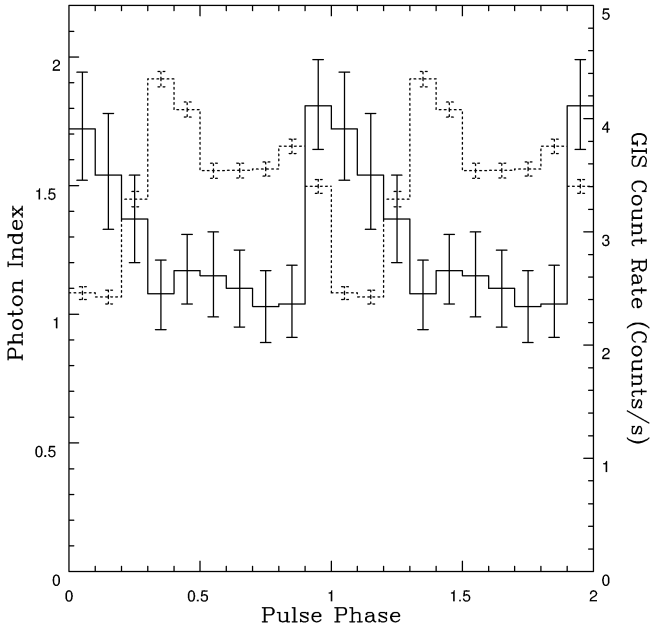

FIG. 7.—Photon spectral index as a function of pulse phase (arbitrary epoch) during Aobs 4. Errors represent the 90% confidence region. The dotted histogram is the GIS count rate.

absorption column *decreases* during the dips, although the statistics on the low flux are such that the data are barely consistent within the 90% multiparameter confidence region. There is no evidence of a significant change in photon index. If we assume that the photon index remains constant, the change in the absorption column is $\sim 2 \times 10^{22}$ cm^{-2}. In the SIS data during the periods of low flux, there appears to be an emission feature near 3.8 keV, which is evident in both the SIS0 and SIS1 data although not apparent in the GIS data. In the GIS data, the fit could be significantly improved by the inclusion of a zero-width Gaussian line at 2.2 keV. This feature appears in several of the data sets, although since it is near the known bump in the response due to gold in the telescopes, this feature should be viewed with caution.

During Aobs 4, the source was only varying by a factor of 2 or so, mostly because of the pulsations, and had a fairly high count rate, allowing tight constraints on $N_{\rm H}$ and the photon index. The fits are significantly improved by the inclusion of an iron line at ~ 6.4 keV. The count rates were sufficiently high during this observation to extract spectra as a function of pulse phase using the best-fit pulse period. There is no strong evidence for variability in $N_{\rm H}$. A strong anticorrelation between the photon index and the intensity is evident, which we show in Figure 7. There also seems to be a concentration of iron line emission in the pulse phase 0–0.1 spectrum. However, the uncertainties in the fitted line strength at the other phases preclude a definitive measurement of line strength variability.

4. *RXTE* OBSERVATIONS

RXTE observed 4U 1907+09 for a second series of observations during 1996 December (observational parameters are listed in Table 3). A total of nine observations (Robs 1–9), each approximately 2 ks in duration, were made spaced roughly 1 day apart in order to evenly sample the 8.4 day orbit. Data from the standard 2 observational mode were analyzed using FTOOLS 4.2. Combined spectra were extracted from all five Proportional Counter Units (PCUs; except Robs 1, which only had PCUs 0–3 on during the observation) and all layers. Model background spectra were then constructed using the background models provided by the *RXTE* Science Operations Facility, which take into account the particle induced background. However, they do not take into account the X-ray background from the Galactic plane. To construct an accurate background model for 4U 1907+09, it is necessary to take into account contributions from both the Galactic ridge and the nearby supernova remnant W49B. During two of the observations, Robs 4 and Robs 5, the source was in the "dip" state. The model background was subtracted from these observations, and their spectra were examined. The count rate of ~ 18 counts s^{-1} is comparable to what is observed by *RXTE* for the diffuse emission from the Galactic ridge (Valinia & Marshall 1998). We created a crude model of the Galactic ridge plus supernova remnant W49B emission consisting of two thermal bremsstrahlung sources with fixed temperatures of 1.8 and ~ 10 keV, moderate (1.6×10^{22} cm^{-2}) absorption, and ~ 6.7 keV Gaussian lines with only the normalizations allowed to vary. These parameter values were taken from Koyama (1989) for this position in the Galactic ridge and Smith et al. (1985) for W49B. This model adequately fitted the data for Robs 4 and Robs 5 with normalizations that could reasonably be expected if the source had dropped to flux levels consistent with the low states seen in the *ASCA* data and if the spectra were dominated by emission from the Galactic ridge and the nearby thermal supernova remnant. Therefore, these observations were used to make a background spectrum for use in spectral fits of the other observations in the following way: Using the background models available from the *RXTE* Guest Observer Facility, we generated background spectra for all

TABLE 3

RXTE OBSERVATION PARAMETERS

Observation	Observation ID	Date (MJD −50,400)	Orbital Phase ($T_{\pi/2} = 0$)	On Time (ks)	Mean Raw PCA Rate (counts s^{-1})
Robs 1.....	10154-02-01	36.40–36.45	0.02	2.4	243
Robs 2.....	10154-02-02	37.39–37.42	0.14	2.4	238
Robs 3.....	10154-02-03	38.39–38.42	0.25	2.4	233
Robs 4.....	10154-02-04	39.39–39.42	0.37	2.4	181
Robs 5.....	10154-02-05	40.39–40.42	0.49	2.4	179
Robs 6.....	10154-02-06	41.05–41.08	0.57	2.5	291
Robs 7.....	10154-02-07	42.06–42.12	0.70	2.6	331
Robs 8.....	10154-02-08	43.06–43.09	0.81	2.4	333
Robs 9.....	10154-02-09	44.05–44.09	0.93	3.3	216

nine observations. These were directly subtracted from the observation spectra using the "Mathpha" FTOOL to create the files to be used in the fitting. The background-subtracted PHA files of Robs 4 and Robs 5 were then added together to create a local X-ray background for 4U 1907+09, which was used as the background file in XSPEC.

All the spectra from the remaining seven observations were modeled using an absorbed power law with a high-energy cutoff in XSPEC. The data were fitted in the energy range of 2.5–20 keV, and the results are listed in Table 4. The measured cutoffs are consistent with the broadband spectral fits of *BeppoSAX* (Cusumano et al. 1998). We also obtained the archival *RXTE* data from 1996 February first analyzed by in 't Zand et al. (1997) to fit for average fluxes and absorption in the 2.5–10 keV band for inclusion in the modeling below.

5. MODELING OF ORBITAL SPECTRAL VARIATIONS

In Figure 8 we show measurements of n_H as a function of the orbital phase for spectral measurements from *ASCA* and *RXTE* (this work), *EXOSAT* (Cook & Page 1987), *Tenma* (Makishima et al. 1984), and *BeppoSAX* (Cusumano et al. 1998). As a consistency check, we also plot the ASM hardness ratio of (5.0–12.1)/(1.3–3.0) keV counts s^{-1} as a function of phase (*dotted line*). Since the spectral slope does not vary greatly, we expect this hardness ratio to change mostly because of the column depth. The vertical lines represent the 68% confidence region of the time of periastron. We see that the absorption begins to increase toward the end of the primary flare and stays high until right before the secondary flare, where it drops again. In Figure 9 we plot the photon spectral index as a function of orbital phase. Small but significant changes are observed. In Figure 10 we plot the 2–10 keV flux measurements from these same observations versus the orbital phase with the ASM light curve overplotted. The secondary flare is twice seen to be nearly as bright as the primary during these observations. One of the *RXTE* observations seen at an overlapping phase with the Aobs 2 is still seen to be moderately bright ($F_X \sim 10^{-10}$ ergs cm^{-2} s^{-1}), although dipping activity is seen during the observation. Therefore, extended periods of low flux as seen in the Aobs 2 and Aobs 3 probably do not occur every orbit. In general, there is a positive flux bias of $\sim$0.1 counts s^{-1} in the ASM data. However, in crowded

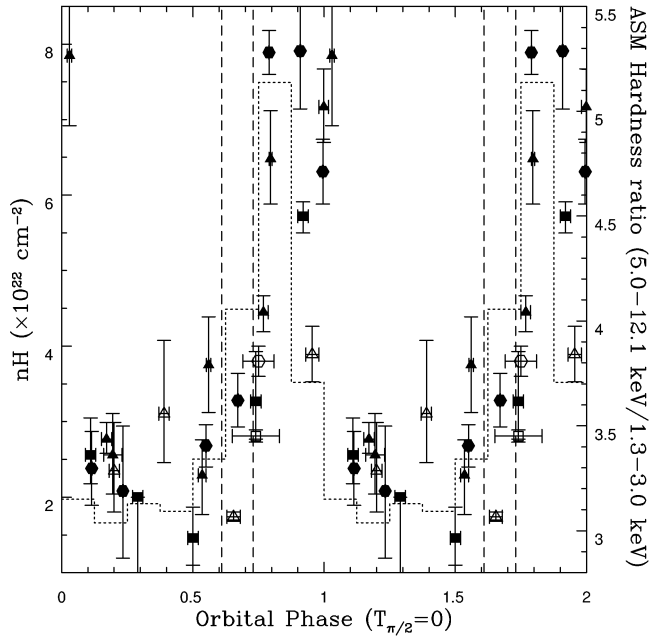

FIG. 8.—Multimission measurement of n_H as a function of orbital phase. Measurements are from *ASCA* (*open triangles*), 1996 February *RXTE* (*filled triangles*), *BeppoSAX* (*open squares*), *EXOSAT* (*filled squares*), *Tenma* (*open hexagons*), and 1996 December *RXTE* (*filled hexagons*). The histogram is the ASM hardness ratio of the count rates from channel 3 over channel 1.

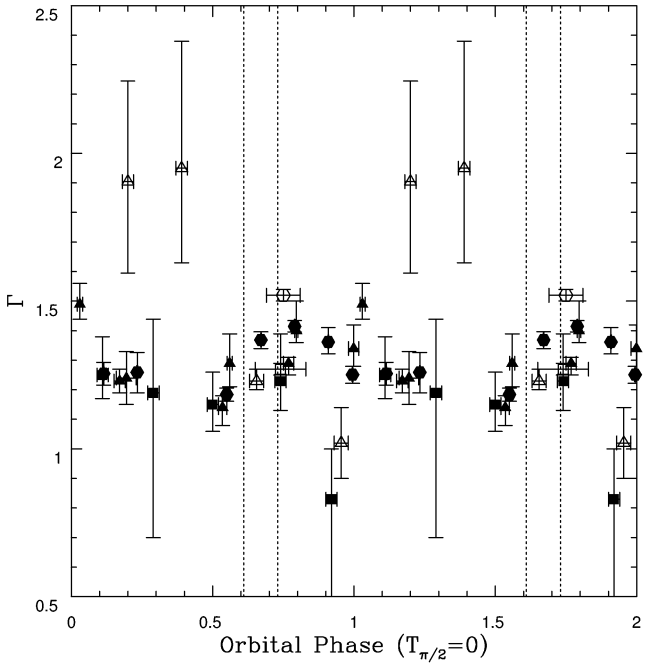

FIG. 9.—Multimission measurement of the photon index as a function of orbital phase.

TABLE 4

RXTE SPECTRAL FITS FROM 1996 DECEMBER OBSERVATIONS

Observation	Phase	n_H ($\times 10^{22}$ cm^{-2})	Γ	Cutoff Energy (keV)	$F_{2-10\,keV}$ ($\times 10^{-10}$ ergs cm^{-2} s^{-1})	χ^2_ν
Robs 1	0.995	$6.31^{+0.43}_{-0.43}$	$1.251^{+0.029}_{-0.029}$	$13.52^{+0.25}_{-0.25}$	2.92	0.63
Robs 2	0.114	$2.38^{+0.49}_{-0.49}$	$1.255^{+0.038}_{-0.039}$	$14.00^{+0.41}_{-0.40}$	1.63	0.84
Robs 3	0.233	$2.08^{+0.86}_{-0.89}$	$1.259^{+0.067}_{-0.070}$	$13.92^{+1.22}_{-0.87}$	0.89	0.92
Robs 6	0.550	$2.68^{+0.28}_{-0.28}$	$1.184^{+0.022}_{-0.023}$	$13.47^{+0.21}_{-0.22}$	3.30	1.00
Robs 7	0.671	$3.28^{+0.36}_{-0.35}$	$1.369^{+0.028}_{-0.029}$	$13.52^{+0.28}_{-0.29}$	4.41	1.50
Robs 8	0.790	$7.89^{+0.29}_{-0.29}$	$1.415^{+0.020}_{-0.019}$	$13.50^{+0.16}_{-0.17}$	4.29	0.88
Robs 9	0.909	$7.91^{+0.81}_{-0.77}$	$1.362^{+0.049}_{-0.048}$	$13.62^{+0.55}_{-0.49}$	1.21	0.72

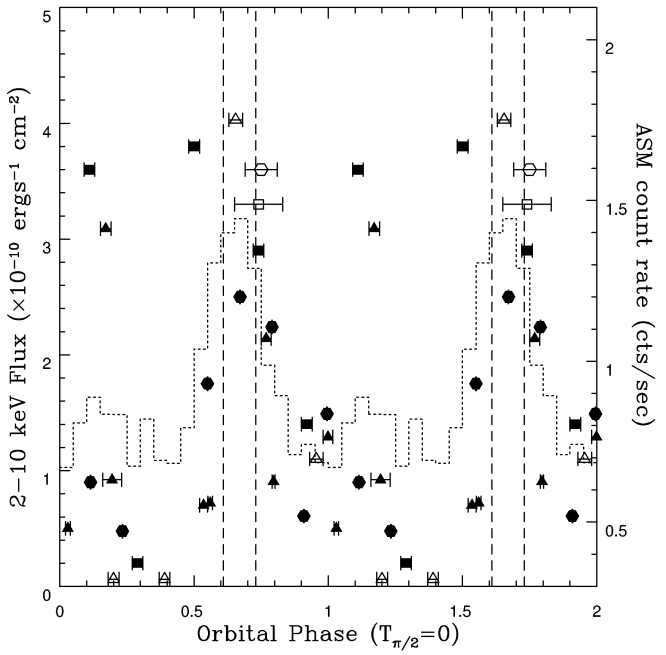

FIG. 10.—Multimission measurement of the 2–10 keV flux as a function of orbital phase. The histogram is the folded light curve from the ASM, with the y-axis starting at the assumed flux bias of 0.3 counts s^{-1}.

regions of the Galactic plane, such as around 4U 1907+09, there are likely to be further systematic biases. By comparing the folded ASM light curve to the observed multimission fluxes, we estimate a positive flux bias of ~0.2–0.6 counts s^{-1}. We will assume a bias of 0.3 for the analysis below.

In this section we model the primary flare and absorption as accretion from a spherical stellar wind with the addition of an absorbing gas stream. This model, first applied to *Tenma* observations of GX 301−2, is detailed in Leahy (1991). We first attempt to model the average ASM light curve and multimission absorption data as accretion from a simple spherical stellar wind with the velocity profile,

$$v_{\rm wind} = v_\infty (1 - R_c/r)^\beta ,$$

where v_∞ is the terminal velocity, assumed to be 3 times the escape velocity, and R_c is the radius of the companion. The Castor, Abbott, & Klein (1975) theoretical wind model has $\beta = 0.5$, but observations of OB stars (Leitherer 1988; Boroson et al. 1999) suggest that $\beta \sim 0.7$–2, depending on spectral type. We assume $\beta = 1$, which is consistent with the assumption of an OB supergiant. In the case of a lower mass Be-type star, models of the wind structure are more complex and uncertain. However, the velocity profile of the polar wind from a Be star is similar to that of an OB supergiant (de Araújo, de Freitas Pacheco, & Petrini 1994), and the profile of the equatorial wind probably has a similar functional form but a lower terminal velocity. If the companion is a Be star, it is likely that the spin axis is not aligned with the orbital axis (see § 6) and so emission dominated by accretion from the polar wind over much of the orbit may not be an unreasonable assumption.

We assume the orbital period $P = 8.3753$ days, a longitude of periastron (i.e., the observer's viewing angle) $\omega = 330°$, and a periastron phase of the best-fit model from in 't Zand et al. (1998) and we fit the ASM light curve for a range of inclination angles by adjusting the eccentricity and the parameter $x = \dot{M}_{20}/d_3^2$, where $\dot{M}_{20}$ is the mass loss rate in units of 10^{20} g s^{-1} and d_3 is the distance in units of 3 kpc. We choose as our canonical values $i = 47.9$, which implies a companion mass $M_c = 24\ M_\odot$ given the mass function derived from the orbital fits assuming a neutron star mass of 1.4 $M_\odot$, and $i = 75.^\circ7$ for a companion mass $M_c = 12\ M_\odot$, which is more in line with a Be star.

For the companion radius, we follow van Kerkwijk et al. (1989) and assume $R_c = 31\ R_\odot$ for a 24 $M_\odot$ star. However, a star of this radius would be larger than its Roche lobe at periastron, as defined in Brown & Boyle (1984), assuming the best-fit eccentricity of $e = 0.28$ (in 't Zand et al. 1998), a rotational velocity $v \sin i = 90$ km s^{-1} (van Kerkwijk et al. 1989), and the alignment of the rotational and orbital axes. In Figure 11 we plot the Roche lobe radius as a function of the companion mass as well as the limits on radius inferred from the lack of eclipses. All supergiant companions would greatly overflow their Roche lobes and would have to be excluded if we assume this as a radius limit. However, a nonrotating (or nonaligned) star has a greater Roche lobe radius, as would a system where the eccentricity is less. For the 12 $M_\odot$ star, we use the Iye (1986) value of $R_c = 6\ R_\odot$ for a Be star companion. For intermediate inclinations and masses, the appropriate radius is dependent on spectral type. For supergiants, the radius actually increases with decreased mass, which would exacerbate the Roche lobe problem. However, type Ib, III, or V stars are all smaller than our canonical Ia supergiant star. In Figure 11 we plot radii for a number of early B stars (Underhill & Doazan 1982). A linearly interpolation between our two canonical stars seems to provide a reasonable mass-radius relationship for modeling purposes.

In Figure 12 we show the range of model curves compared to the ASM light curve. To fit the higher mass companion to the shape of the primary flare an eccentricity,

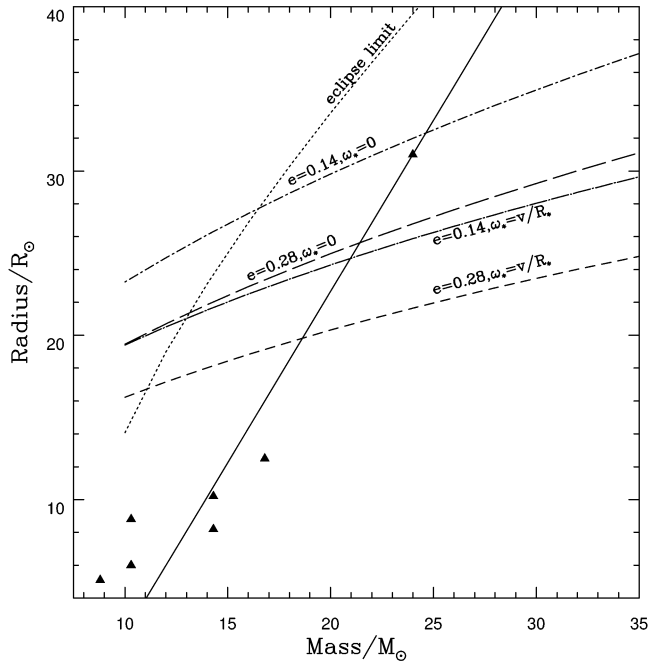

FIG. 11.—Assumed mass/radius relationship (*solid line*) compared to eclipse limit and periastron "Roche lobe" radii assuming different eccentricities and stellar rotation rates in the orbital plane (Ω_*). Points are various stellar values for main-sequence, giant, and supergiant B0–B3 stars (Underhill & Doazan 1982).

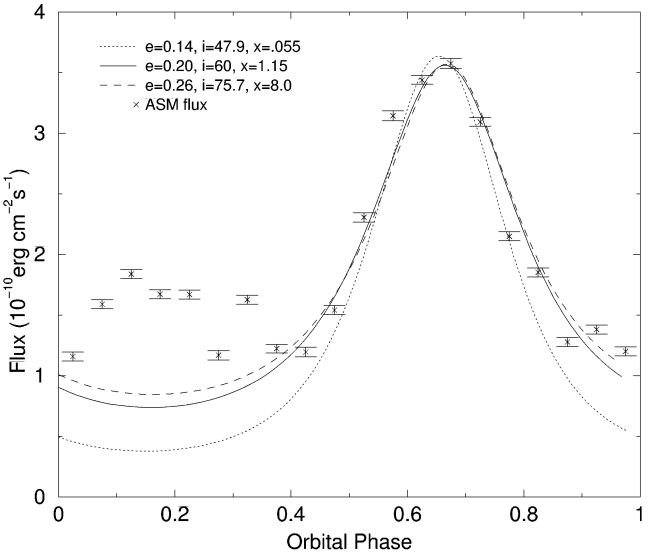

FIG. 12.—Spherical wind model fits to ASM light curve assuming inclination angles of 47°.9 ($M_c = 24\ M_\odot$), 60° ($M_c = 16\ M_\odot$), and 75°.7 ($M_c = 12\ M_\odot$).

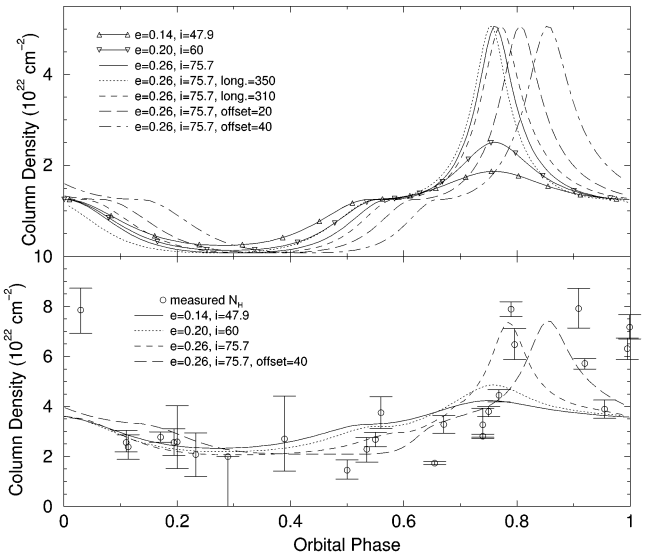

FIG. 14.—Absorption due to a trailing gas stream. *Top*: Orbital variation of absorption due to the stream for various parameters. *Bottom*: Wind plus stream absorption model compared to the multimission measurements of n_H.

$e \lesssim 0.14$ is required (which would also allow the star to underfill its Roche lobe at periastron). For the lower mass companion, the best fit to the observed primary flare peak is $e = 0.26$, more in line with the best-fit eccentricity from the pulse arrival analysis. In no case can a secondary flare be produced from this model.

This luminosity model implies a varying absorption as a function of orbital phase, with the overall normalization being only a function of $\dot{M}$. Using the parameters given above and an assumed interstellar absorption of $n_H = 1.5 \times 10^{22}$ cm^{-2}, we find that $\dot{M}_{20} = 1$–1.5 best fitted the absorption data over our range of inclination angles. This is somewhat low for a B supergiant but quite high for a Be star (de Araújo et al. 1994). In order to improve the fit, we also vary the longitude of periastron since it is poorly constrained by the pulse arrival time analysis of in 't Zand et al. (1998). In Figure 13 we plot the results compared to the multimission data. Neither the phase nor the amplitude of the large increase in the absorption after periastron can be produced from this simple spherical wind model.

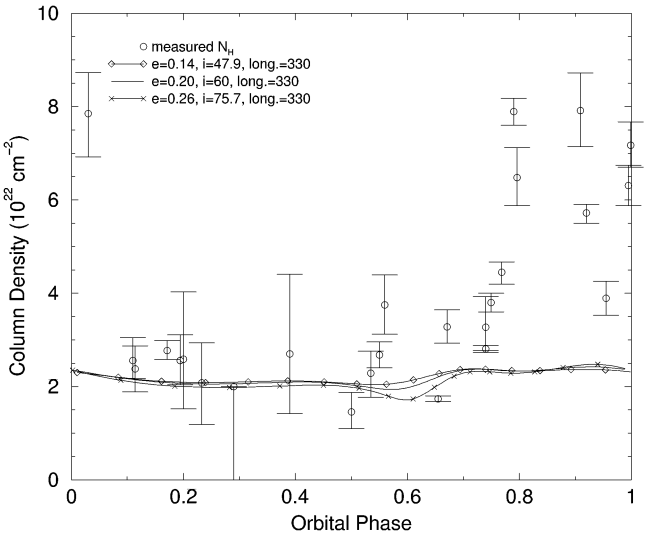

FIG. 13.—Spherical wind model absorption compared with multimission spectral fits.

We can use the $\dot{M}$ from the absorption fits and the parameter x from the luminosity model to estimate distances to the system. For the 24 $M_\odot$ model, we derive a distance $d \sim 4.3$ kpc, while for the 16 and 12 $M_\odot$ models, we derive $d \sim 1.0$ and $d \sim 0.4$ kpc, respectively. The first is in line with the distance estimates of 5.9–2.4 kpc for a supergiant companion from van Kerkwijk et al. (1989), and the latter are consistent with their estimates of 1.5–0.6 kpc for a giant. Note that the minimum measured $n_H \sim 1.5 \times 10^{22}$ cm^{-2} means that the assumed interstellar component of the absorption is an upper limit. Thus, the derived values of $\dot{M}$, and hence the inferred distances, should be considered lower limits.

To fit the postperiastron absorption, we added a linear trailing gas stream to the above model (see Leahy 1991 for details). Such a stream can be interpreted as arising from the wake caused by the passage of the neutron star through the wind or from an accretion stream coming from the companion (although this latter interpretation would require modification of the luminosity model). The stream is modeled as a density enhancement with a Gaussian profile perpendicular to the stream line, an exponential cutoff on the front side, and no cutoff in the downstream direction. The total contribution to the absorption is then obtained by integrating along the line of site. For a given orbital phase, longitude of periastron, and orbital inclination, the amplitude of the absorption enhancement of the trailing gas stream is completely determined by the product $n_0 \sigma \sim 10^{22}$ cm^{-2}, where n_0 is the central density and σ the Gaussian width. The additional absorption due to the stream is shown in the top of Figure 14. The phase of the absorption peak is somewhat earlier than indicated by the data, so we also tried offsetting the stream line toward the companion star by angles of 20° and 40°. The bottom panel of Figure 14 shows how the combined wind plus stream model compares to the absorption data for the various cases. We find that an adequate fit can be obtained with the larger inclination

angles and an offset stream. A downstream cutoff of the stream would tend to broaden the peak somewhat, which might further improve the fit.

6. DISCUSSION

If the eccentricity of $e \gtrsim 0.2$ of the best-fit orbital parameters from pulse arrival time analyses is correct, the primary flare seen in the overall light curve can be fitted using a model of accretion from a spherical wind off of a star of mass $M_c \lesssim 16\ M_\odot$. However, the absorption measurements and the persistence of the secondary flare require modifications to this model. We have shown that a trailing accretion stream moderately offset toward the companion can account for the extra absorption component although not the secondary flare. Such an offset stream may be indicated by the high-resolution, two-dimensional hydrodynamical simulations of Benensohn, Lamb, & Taam (1997). The "flip-flop" instability seen in their simulations modifies the direction of the downstream flow so that it switches back and forth, resulting in a wake that could be characterized by two offset streams, one of which could provide the enhanced absorption seen in the data (see Fig. 2 of Benensohn et al. 1997). This instability can in principle also explain the "dipping" or "flaring" behavior seen in Aobs 1 and in the *RXTE* observations of in 't Zand et al. (1997) and may even be compatible with a drop in absorption during low-accretion phases. However, this instability may just be an artifact of two-dimensional simulations, and whether similar affects occur in a three-dimensional flow is an open question. Recent three-dimensional simulations by Ruffert (1999) do exhibit active unstable phases, although the changes in the accretion rate tend to be smaller, and the downstream density profile is unclear.

The spherical wind accretion models favor a high inclination angle, implying a companion mass more in line with a Be star than a supergiant. In addition, if the companion mass is high, the models imply an eccentricity near the low end of the acceptable range. This lower eccentricity is also required to keep a massive supergiant from greatly overflowing its Roche lobe near periastron. Even with a smaller eccentricity, it is likely that periodic Roche lobe overflow (Brown & Boyle 1984) or tidal stripping (Layton et al. 1997) would be the dominant mass transfer mechanism. In this case, the observed accretion rate and orbital variation may be somewhat low unless long-term storage of material by an accretion disk could keep the accretion rate low except for occasional large outbursts like the one seen by *Ariel 5* in 1980 (Marshall & Rickets 1980). If the best-fit eccentricity value of $e \sim 0.28$ is correct, it would seem to exclude the accretion from a supergiant wind model. This suggests that an alternative model of the accretion perhaps should be considered. One persistent possibility is an equatorially enhanced wind with the neutron star in an inclined orbit, as suggested by Iye (1986). In this case, the neutron star passes behind an extended-matter disk around the companion after periastron and comes back through after apastron. While tidal forces would tend to align the neutron star orbital axis with that of the companion's spin axis, the timescale for this is similar to the circularization timescale, and accretion processes might counteract the tidal forces somewhat (Matese & Whitmire 1983). Given that the orbit is eccentric, we do not view a somewhat inclined orbital axis as being unreasonable.

In the equatorially enhanced wind scenario, the flares are fed by matter gathered by the neutron star as it passes through the matter envelope. If the outflow speed is somewhat slower near the equator, the size of this envelope might be limited by the neutron star's orbit. Such truncation is indicated from studies of the Hα emission line in several Be/X-ray binary systems (Zamanov et al. 2001). The matter is depleted by the periastron passage of the neutron star, so significantly less material is available further out at the apastron radius. If sufficiently depleted, there may be no secondary flare at all. Hence, we get an intermittent but phase-locked secondary flare.

The major difficulty to this picture is the "virtually certain" classification of the companion as a supergiant by van Kerkwijk et al. (1989). This is based on a collection of observed properties of the system, with some favoring a Be star and some favoring a supergiant. Two factors seem to greatly favor the supergiant interpretation. First is the color excess $E_{B-V} = 3.4 \pm 0.2$, which is quite high for the inferred distance of $\lesssim 1.5$ kpc of a Be star. However, the variation in the absorption column with the orbital phase suggests that much of this could be local. Indeed, the average excess determined from interstellar absorption lines is only $E_{B-V} = 2.4 \pm 0.5$ or $E_{B-V} = 2.7 \pm 0.6$, depending on which coefficients for the ratio of equivalent width to color excess are used (van Kerkwijk et al. 1989). These lower values are more in line with the inferred interstellar X-ray absorption of $n_{\rm H} \lesssim 1.5 \times 10^{22}$ cm^{-2}. The independent distance estimate that van Kerkwijk et al. 1 (1989) obtain from the interstellar sodium lines of $d = 2.1 \pm 0.6$ is between the supergiant and Be star distances and consistent with both given the error.

The second factor strongly favoring the supergiant interpretation is the large FWHM ~ 700 km s^{-1} of the Hα line combined with the relatively low projected rotational velocity $v \sin i \sim 90$ km s^{-1}. While neither value is exceptionally unusual for a Be star, the combination is (Dachs et al. 1986). The inclination angle suggested by the observed projected rotational velocity is $i \sim 15^\circ$ assuming typical Be star rotational velocities, as opposed to the inferred orbital inclination $i \sim 60^\circ$–75° of the neutron star with a giant or main-sequence star companion, consistent with the inclined orbit scenario. However, the large value of the FWHM suggests that the outflowing disk is seen nearly edge on. The circumstellar envelope can and would be affected by the neutron star, as evidenced by the large-scale perturbations observed in the Hα profiles of several Be/X-ray binaries (Negueruela et al. 1998). Since the orbital period of 4U 1907+09 is shorter than any of the known Be/X-ray binaries (except A0538−66, which is not well observed), it would be expected to have a much greater perturbing effect. It is interesting to note that the projected orbital velocity of a particle in the orbital plane near the Roche lobe radius of a lower mass star in 4U 1907+09 is roughly half the observed Hα FWHM. If the gravitational attraction of the neutron star could warp the equatorial outflow of the companion such that it would be nearly coplanar to the neutron star orbit at the Roche lobe radius, the observed FWHM might result. Hydrodynamical simulations should be able to determine if such a scenario is feasible.

The relatively long periods of low accretion rate seen in Aobs 2 and Aobs 3 are somewhat puzzling. Inhomogeneities in the wind from the companion could possibly account for these variations, although the apparent dura-

tion of several days during the *ASCA* observations would argue against this. If the accretion is modified by a transient accretion disk, instabilities in the accretion disk could account for both the sudden changes in accretion rate seen in Aobs 1 and the longer periods of quiescence seen in Aobs 2 and Aobs 3. The consistent spin-up of the neutron star and the 18 s oscillations seen by *RXTE* (in 't Zand et al. 1997) argue for the existence of an accretion disk. The on-off behavior seen by both *RXTE* and *ASCA* are suggestive of magnetically inhibited accretion from a disk whose inner edge is near the corotation radius. The residual emission during the off periods may then be a result of accretion on to the magnetosphere or a bow shock. However, the slow spin period and correspondingly large corotation radius makes this unlikely.

7. COMPARISON WITH GX 301−2

4U 1907+09 is similar in many respects to the wind-fed supergiant/X-ray pulsar binary system GX 301−2. Both have eccentric orbits and occupy a similar location on the spin period versus orbital period diagram (Corbet 1986; for GX 301−2, $e \sim 0.47$, $P_{\rm spin} \sim 680$ s, and $P_{\rm orb} \sim 41.5$ days; see Koh et al. 1997). The absorption profile and primary orbital flux peak of both systems have been successfully fitted by a spherical wind plus gas stream model (Leahy 1991). GX 301−2 also has extended periods where there is a secondary orbital flare at a consistent phase that cannot be fitted by wind models. An equatorially enhanced outflow has also been suggested for this system, and models of such an outflow can grossly fit the orbital light curve (Koh et al. 1997). Both systems have companions with similar temperatures (spectral type B2) and projected rotational velocities ($v \sin i \sim 70$ for GX 301−2; Parkes et al. 1980).

However, the companion star of GX 301−2, Wray 977, is unambiguously identified as a supergiant by the strength of various lines in the blue portion of the spectrum (Parkes et al. 1980). The observations of Iye (1986) and van Kerkwijk et al. (1989) did not extend into the blue portion of the spectrum, so such diagnostics are not available for 4U 1907+09. The Hβ emission line of Wray 977 has a P Cygni profile (Parkes et al. 1980), which is clear evidence of an expanding atmosphere. No such profiles have been seen in 4U 1907+09.

The local absorption column and iron line equivalent width of the X-ray spectrum of GX 301−2 are both more than an order of magnitude stronger than in 4U 1907+09. This implies that the mass loss from Wray 977 is much greater than from the companion of 4U 1907+09 despite the similarity in the proposed spectral classes. While enhanced mass loss in these systems could be expected because of gravitational interaction with a neutron star, the orbit of GX 301−2 is significantly wider, and there is no question that the companion remains inside its Roche lobe (although at periastron it can come close; Leahy 1991). If both were supergiants, the naive expectation would be greater mass loss from the companion of 4U 1907+09 due to transient Roche lobe overflow (Brown & Boyle 1984) or tidal stripping Layton et al. (1997).

The changes in the spectral index with the pulse phase of both systems show a softening of the spectrum near the pulse minimum in the 1–10 keV band (Saraswat et al. 1996; Leahy & Matsuoka 1990). The iron line equivalent width in GX 301−2 varies with pulse phase as well, with a peak near the pulse minimum. The possible iron line enhancement near the pulse minimum in the 4U 1907+09 *ASCA* data, if real, would be consistent. These similarities in the phase-resolved spectra suggest that the accretion columns are similar. This is not surprising since the spin periods and surface magnetic field strengths (as inferred from their cyclotron absorption lines) are similar.

8. CONCLUSIONS

Observations of the variation of the spectra of 4U 1907+07 with the orbital phase are consistent with a simple spherical wind accreting onto the neutron star from an OB supergiant companion with excess absorption caused by a trailing accretion wake. However, the implied inclination angle for such a model suggests a relatively low mass ($\lesssim 16\ M_\odot$) for the companion. The excess of the absorption column seen after periastron might also be interpreted as the neutron star passing through an equatorially enhanced matter envelope in an inclined orbit. Observations of the secondary flare near apastron by *RXTE* and *HEAO 1* A-1, as well as the average orbital light curve from the *RXTE* ASM, further support the hypothesis that this flaring has been occurring at a consistent phase but with a variable amplitude for 20 yr. The measurements of the low states by *ASCA* suggest that the accretion rate can change by 1–2 orders of magnitude over a short time period, perhaps because of a transient accretion disk. The most critical components to a better understanding of this system are more secure measurements of the orbital eccentricity and periastron phase and improved optical measurements of the companion. A high-resolution optical spectrum at shorter wavelengths and orbital radial velocity measurements could unambiguously determine the companion type.

We thank J. G. Jernigan for useful discussions as to the nature of the companion star in this system and the anonymous referee for pointing out the importance of the Roche lobe radius. ASM results were provided by the *RXTE* ASM teams at MIT and at the *RXTE* Science Operations Facility and Guest Observer Facility at NASA's GSFC. This work was supported in part by NASA Guest Observer grants NAG 5-2948 and NAG 5-3332.

REFERENCES

Benensohn, J. S., Lamb, D. Q., & Taam, R. E. 1997, ApJ, 478, 723
Boroson, B., Kallman, T., McCray, R., Vrtilek, S. D., & Raymond, J. 1999, ApJ, 519, 191
Brown, J. C., & Boyle, C. B. 1984, A&A, 141, 369
Castor, J. I., Abbott, D. C., & Klein, R. I. 1975, ApJ, 195, 157
Chitnis, V. R., Rao, A. R., Agrawal, P. C., & Manchanda, R. K. 1993, A&A, 268, 609
Collura, A., Maggio, A., Sciortino, S., Serio, S., Vaiana, G. S., & Rosner, R. 1987, ApJ, 315, 340
Cook, M. C., & Page, C. G. 1987, MNRAS, 225, 381
Corbet, R. 1984, A&A, 141, 91
———. 1986, MNRAS, 220, 1047
Cusumano, G., Di Salvo, T., Burderi, L., Orlandini, M., Piraino, S., Robba, N., & Santangelo, A. 1998, A&A, 338, L79
Dachs, J., Hanuschik, R., Kaiser, D., & Rohe, D. 1986, A&A, 159, 276
de Araújo, F. X., de Freitas Pacheco, J. A., & Petrini, D. 1994, MNRAS, 267, 501
Giacconi, R., Kellogg, E. Gorenstein, P., Gursky, H., & Tananbaum, H. 1971, ApJ, 165, L27
in 't Zand, J. J. M., Baykal, A., & Strohmayer, T. E. 1998, ApJ, 496, 386
in 't Zand, J. J. M., Strohmayer, T. E., & Baykal, A. 1997, ApJ, 479, L47
Iye, M. 1986, PASJ, 38, 463
Koh, D. T., et al. 1997, ApJ, 479, 933
Koyama, K. 1989, PASJ, 41, 665

Layton, J. T., Blondin, J. M., Owen, M. P., & Stevens, I. R. 1997, NewA, 3, 111
Leahy, D. A. 1991, MNRAS, 250, 310
Leahy, D. A., & Matsuoka, M. 1990, ApJ, 355, 627
Leitherer, C. 1988, ApJ, 326, 356
Makishima, K., Kawai, N., Koyama, K., & Shibazaki, N. 1984, PASJ, 36, 679
Makishima, K., Mihara, T., Nagase, F., & Tanaka, Y. 1999, ApJ, 525, 978
Markert, T. H., et al. 1979, ApJS, 39, 573
Marshall, N., & Ricketts, M. J. 1980, MNRAS, 193, 7P
Matese, J. J., & Whitmire, D. P. 1983, ApJ, 266, 776
Mihara, T. 1995, Ph. D. thesis, Univ. Tokyo
Negueruela, I., Reig, P., Coe, M. J., & Fabregat, J. 1998, A&A, 336, 251
Parkes, G. E., Mason, K. O., Murdin, P. G., & Culhane, J. L. 1980, MNRAS, 191, 547
Pravdo, S. H., Day, C. S. R., Angelini, L., Harmon, B. A., Yoshida, A., & Saraawat, P. 1995, ApJ, 454, 872
Priedhorsky, W. C., & Terrell, J. 1984, ApJ, 280, 661
Ruffert, M. 1999, A&A, 346, 861
Saraswat, P., et al. 1996, ApJ, 463, 726
Schwartz, D. A., Griffiths, R. E., Thorstensen, J. R., Charles, P. A., & Bowyer, S. 1980, AJ, 85, 549
Seward, F. D., Page, C. G., Turner, M. J. L., & Pounds, K. A. 1976, MNRAS, 175, 39P
Smith, A., Peacock, A., Jones, L. R., & Pye, J. P. 1985, ApJ, 296, 469
Underhill, A. B., & Doazan, V. 1982, B Stars with and without Emission Lines (NASA SP-456; Washington, DC: NASA)
Valinia, A., & Marshall, F. E. 1998, ApJ, 505, 134
van Kerkwijk, M. H., van Oijen, J. G. J., & van den Heuvel, E. P. J. 1989, A&A, 209, 173
Zamanov, R. K., Reig, P., Martí, J., Coe, M. J., Fabregat, J., Tomov, N. A., & Valchev, T. 2001, A&A, 367, 884